Supporting information

Combinatorial screening yields discovery of 29 metal oxide photoanodes for solar fuel generation

Summary of photoanodes in high throughput experiments

The identification of 58 photoanode phases in the high throughput dataset proceeded as follows: (i) mining all toggled illumination chronoamperometry experiments at 1.23 V vs RHE, (ii) selecting samples that meet phase purity requirements from XRD measurements, (iii) aggregating by phase by taking maximum photocurrent over set of corresponding samples for each illumination source, (iv) choosing the representative pH as that with maximum photocurrent under 3.2 eV illumination, (v) applying photocurrent thresholds, (vi) manual inspection of edge cases and samples containing a minority phase that may be photoactive. The resulting table of 58 phases has a representative electrolyte pH for each phase and the photocurrent and corresponding EQE values under 4 LED (3.2, 2.7, 2.4, and 2.1 eV) illumination, as shown in Table S1.

Table S1. Photoelectrochemical (PEC) data for 58 phases identified as photoanodes in ternary oxide libraries ($A_{1-x}B_xO_z$, where B is the higher valent cation) via high throughput experimentation. The corresponding EQE values at 4 different LED illumination sources are provided, where NA refers to lack of PEC data. Sorting is by decreasing EQE value at 2.4 eV illumination, and different illumination intensities result in non-monotonic lowering of the photocurrent.

formula	mp id	pH	3.2 eV light source			2.7 eV light source			2.4 eV light source			2.1 eV light source		
			EQE (%)	Iphoto (μA)	LED power (mW)	EQE (%)	Iphoto (μA)	LED power (mW)	EQE (%)	Iphoto (μA)	LED power (mW)	EQE (%)	Iphoto (μA)	LED power (mW)
$FeWO_4$	19421	9	2.018	17.7	2.81	1.514	14	2.52	1.398	5.7	0.98	0.081	0.269	0.68
α-$V_2Cu_2O_7$	505508	7	3.781	32.8	2.794	1.55	7.55	1.331	0.316	0.842	0.623	0.007	0.048	1.33
γ-$V_2Cu_3O_8$	504747	13	6.180	52.9	2.96	1.24	10.95	2.47	0.248	1.13	1.17	0.021	0.263	2.46
$Y_3Fe_5O_{12}$	19648	13	0.892	5.96	2.14	0.389	2.71	1.9	0.156	0.51	0.786	0.012	0.028	0.50
β-VAg_3O_4	19412	9	0.793	7.29	2.96	0.287	2.47	2.37	0.103	0.41	0.96	0	0	0.8
$FeBiO_3$	24932	9	0.405	3.55	2.81	0.152	1.41	2.52	0.087	0.357	0.98	0.018	0.061	0.68
V_2CoO_6-tri	622217	9	0.109	1	2.96	0.073	0.628	2.37	0.069	0.274	0.96	0	0	0.8
$VBiO_4$	504878	9	2.872	26.4	2.96	0.905	7.8	2.37	0.051	0.203	0.96	0	0	0.8
$SrMnO_3$	568977	13	1	9.23	2.958	0.24	2.08	2.37	0.022	0.088	0.96	0	0	0.8
$YFeO_3$-orth	24999	13	0.086	0.571	2.14	0.06	0.416	1.9	0.021	0.069	0.79	0	0	0.5
$BaMnO_3$	19156	13	0.374	3.45	2.958	0.040	0.345	2.37	0.020	0.08	0.96	0	0	0.8
$VFeO_4$	540630	9	2.470	22.7	2.96	0.205	1.77	2.37	0.013	0.053	0.96	0	0	0.8
YMn_2O_5	542867	10	0.025	0.167	2.1	0.022	0.163	2	0.013	0.042	0.8	0.004	0.010	0.5
$YMnO_3$-hex	19227	13	0.018	0.118	2.14	0.015	0.106	1.9	0.013	0.043	0.79	0.007	0.018	0.5
β-$VAgO_3$	566337	9	0.056	0.512	2.96	0.012	0.106	2.37	0.011	0.044	0.96	0	0	0.8
α-VAg_3O_4	18889	9	0.184	1.69	2.96	0.018	0.156	2.37	0.007	0.028	0.96	0.011	0.042	0.8
$V_2Ag_{0.333}O_5$	none	9	0.089	0.586	2.1	0.013	0.099	2	0.001	0.004	0.8	0	0	0.5
$V_4Cr_2O_{13}$	851269	9	0.267	2.45	2.96	0.054	0.467	2.37	0	0	0.96	0	0	0.8
$VCrO_4$-orth	19418	9	0.696	6.4	2.96	0.073	0.633	2.37	0	0	0.96	0	0	0.8
$V_2Ni_3O_8$	542151	9	0.006	0.058	2.96	0.006	0.0475	2.37	0	0	0.96	0	0	0.8
$NbVO_5$	769890	9	0.704	6.47	2.96	0.003	0.023	2.37	0	0	0.96	0	0	0.8
$V_2Bi_4O_{11}$	767756	9	0.490	4.5	2.96	0.145	1.25	2.37	0	0	0.96	0	0	0.8
$Nb_{10.7}V_{2.38}O_{32.7}$	none	9	0.179	1.65	2.96	0.001	0.013	2.37	0	0	0.96	0	0	0.8
$V(Bi_5O_8)_5$	none	9	0.022	0.2	2.958	0.004	0.031	2.37	0	0	0.96	0	0	0.8
$V_{4.51}Pb_{3.5}O_{14.75}$	none	9	0.007	0.063	2.96	0.004	0.032	2.37	0	0	0.96	0	0	0.8
V_2CoO_6-mono	773310	9	0.029	0.263	2.96	0.014	0.121	2.37	0	0	0.96	0	0	0.8
$YFeO_3$-hex	3556	13	0.032	0.215	2.14	0.001	0.010	1.9	0	0	0.786	0	0	0.5

$V_2Pb_4O_9$	647385	9	0.030	0.274	2.96	0.001	0.013	2.37	0	0	0.96	0	0	0.8
Ca_2MnO_4	19050	10	0.056	0.367	2.1	0.047	0.342	2	0	0	0.8	0	0	0.5
$V_2Co_3O_8$	540833	9	0.013	0.124	2.958	0.022	0.192	2.37	0	0	0.96	0	0	0.8
V_2ZnO_6	551601	9	0.067	0.618	2.958	0.002	0.017	2.37	0	0	0.96	0	0	0.8
$Ca_2Mn_3O_8$	18893	13	0.338	2.26	2.14	0.102	0.712	1.9	0	0	0.79	0	0	0.5
$CaMnO_3$	19201	13	0.091	0.838	2.96	0.019	0.165	2.37	0	0	0.96	0	0	0.8
$V_2Ni_2O_7$	557404	9	0.006	0.054	2.96	0	0	2.37	0	0	0.96	0	0	0.8
Fe_2WO_6	25749	3	0.009	0.067	2.4	0	0	1.8	0	0	0.77	0	0	0.54
$TaVO_5$	32407	9	0.016	0.145	2.958	0	0	2	0	0	0.8	0	0	0.5
$V_2Bi_{12}O_{23}$	none	9	0.003	0.032	2.96	0	0	2.37	0	0	0.96	0	0	0.8
$V_2Pb_2O_7$	25796	9	0.031	0.285	2.958	0	0	2	0	0	0.8	0	0	0.5
$V_2Zn_4O_9$	504923	9	0.133	1.22	2.96	0	0	2.37	0	0	0.96	0	0	0.8
$YMnO_3$-orth	25025	13	0.062	0.576	2.958	0	0	2	0	0	0.8	0	0	0.5
ZrV_2O_7	565725	9	0.009	0.084	2.96	0	0	2.37	0	0	0.96	0	0	0.8
$V_2Bi_8O_{17}$	none	9	0.004	0.040	2.96	NA	NA	NA	NA	NA	NA	NA	NA	NA
$Ca_2V_2O_7$	32434	9	0.013	0.129	3.248	NA	NA	NA	NA	NA	NA	NA	NA	NA
$CaMn_3O_6$	566229	10	0.203	1.864	2.96	NA	NA	NA	NA	NA	NA	NA	NA	NA
Mg_2MnO_4	none	10	0.213	1.73	2.6	NA	NA	NA	NA	NA	NA	NA	NA	NA
Mg_6MnO_8	19239	10	0.249	2.02	2.6	NA	NA	NA	NA	NA	NA	NA	NA	NA
$Mn_{2/3}Sb_{4/3}O_4$	763546	0	0.037	0.473	4.1	NA	NA	NA	NA	NA	NA	NA	NA	NA
Mn_7SiO_{12}	19650	13	0.025	0.231	2.958	NA	NA	NA	NA	NA	NA	NA	NA	NA
$MnGeO_3$	643577	13	0.005	0.049	2.958	NA	NA	NA	NA	NA	NA	NA	NA	NA
$SrMn_3O_6$	none	10	0.259	2.1	2.6	NA	NA	NA	NA	NA	NA	NA	NA	NA
$MgMn_2O_4$	32006	10	0.195	1.58	2.6	NA	NA	NA	NA	NA	NA	NA	NA	NA
$Mn(Ni_3O_4)_2$	19442	10	0.006	0.052	2.6	NA	NA	NA	NA	NA	NA	NA	NA	NA
$V_2(CuO_2)_5$	559440	9	0.362	3.33	2.96	NA	NA	NA	NA	NA	NA	NA	NA	NA
$V_6Cu_{11}O_{26}$	505456	9	3.307	30.4	2.96	NA	NA	NA	NA	NA	NA	NA	NA	NA
$Zn(FeO_2)_2$	19313	10	1.027	5.26	1.65	NA	NA	NA	NA	NA	NA	NA	NA	NA
α-V_2CuO_6	741706	9	1.839	16.9	2.96	NA	NA	NA	NA	NA	NA	NA	NA	NA
β-$V_2Cu_2O_7$	559660	13	4.411	51.5	3.76	NA	NA	NA	NA	NA	NA	2.540	31.1	2.46
$VCrO_4$-mono	17831	9	0.057	0.521	2.96	NA	NA	NA	NA	NA	NA	NA	NA	NA

Experimental details

PVD library synthesis

The ternary oxide composition libraries were fabricated using RF/DC magnetron co-sputtering onto 100 mm-diameter Si (with Pt conducting layer) or glass (Pyrex or soda lime glass with SnO_2:F conducting layer) substrate in a custom-designed combinatorial sputtering system (Kurt J. Lesker, CMS24) described in detail previously.[1] All depositions used 2" metal sputter targets, with the exception of the Ag-containing libraries, which used an Ag_2O target. The composition libraries were either deposited as "metal" or "oxide" thin films, referring to the absence or presence of the reactive O_2 in the chamber. The deposition pressure was controlled at 6 mTorr of mostly Ar with the O_2 pressure noted in Table S2. The non-confocal geometry of the deposition sources resulted in the composition gradients in the co-sputtered continuous composition spread. The power applied on each source was adjusted according to the deposition rate and desired composition range. The film thickness was not measured for each composition library but was estimated to be 200 nm based on the deposition rate calibration assuming the average molar density of the elemental oxides. The as-deposited composition libraries were subsequently placed flat on a quartz support and annealed in a Thermo Scientific box oven in flowing air at various temperatures and durations. Table S2 summarized the deposition and annealing conditions for the 29 photoanode phases identified by high throughput experimentation in the present work.

Table S2. Physical vapor deposition and annealing conditions are listed for 29 ternary oxide photoanode phases discovered in the present work. All depositions used metal targets with the exception of the Ag-containing libraries, which used an Ag_2O target. RF power supplies were used for all sources except those noted DC power.

Phase name	mp-id	Substrate	Deposition conditions			Annealing conditions	
			O_2 partial pressure (mTorr)	power (W)	power (W)	Temp. (°C)	Duration (hrs)
V_2CoO_6-tri	622217	FTO/Tec7	0	Co: 24	V: 152	550	3
$Y_3Fe_5O_{12}$	19648	Pt/Ti/SiO_2/Si	0.9	Fe: 52	Y: 150	850	3
$YMnO_3$-hex	19227	Pt/Ti/SiO_2/Si	0	Mn: 66	Y: 100	850	3
$YFeO_3$-orth	24999	Pt/Ti/SiO_2/Si	0.9	Fe: 52	Y: 150	850	3
$CaMnO_3$	19201	Pt/Ti/SiO_2/Si	0.12	Ca: 77	Mn: 150	850	3
$V(Bi_5O_8)_5$	none	FTO/Tec7	0.6	Bi: 14	V: 175	550	3
$Nb_{10.7}V_{2.38}O_{32.7}$	none	FTO/Tec7	0.6	Nb: 76	V: 150	550	1
$NbVO_5$	769890	FTO/Tec7	0.6	Nb: 76	V: 150	550	1
$V_2Pb_4O_9$	647385	FTO/Tec7	0	Pb: 29	V: DC, 150	550	3
V_2ZnO_6	551601	FTO/Tec7	0.6	Zn: 14	V: 175	550	3
$V_{4.51}Pb_{3.5}O_{14.75}$	none	FTO/Tec7	0	Pb: 29	V:DC, 150	300	10
β-$VAgO_3$	566337	FTO/Tec7	1.2	Ag_2O, 30	V: 180	300	10
Ca_2MnO_4	19050	Pt/Ti/SiO_2/Si	0.12	Ca: 77	Mn: 150	850	3
Mn_7SiO_{12}	19650	Pt/Ti/SiO_2/Si	0.9	Si: 52	Mn: 150	1100	3
$V_2Bi_{12}O_{23}$	none	FTO/Tec7	0.6	Bi: 14	V: 175	550	3
$YMnO_3$-orth	25025	Pt/Ti/SiO_2/Si	0.9	Mn: 100	Y: 150	850	3
$V_2Ag_{0.333}O_5$	none	FTO/Tec7	1.2	Ag_2O, 30	V: 180	300	10
YMn_2O_5	542867	Pt/Ti/SiO_2/Si	0	Y: 100	Mn: 66	850	3
$Mn_{(2/3)}Sb_{(4/3)}O_4$	763546	FTO/XG	0.6	Sb: 42	Mn: 142	700	3
$Ca_2V_2O_7$	32434	FTO/Tec15 Pyrex	0	Ca:DC, 93	V: DC, 150	550	3
$CaMn_3O_6$	566229	Pt/Ti/SiO_2/Si	0.3	Ca: 150	Mn:DC, 36	850	3
Mg_6MnO_8	19239	Pt/Ti/SiO_2/Si	0.12	Mg: 110	Mn: 120	850	3
$SrMn_3O_6$	none	Pt/Ti/SiO_2/Si	0.12	Sr: 130	Mn: 90	850	3
$MnGeO_3$	643577	Pt/Ti/SiO_2/Si	0.9	Mn: 150	Ge: 40	900	3
$V_2Bi_8O_{17}$	none	FTO/Tec7	0.6	Bi: 20	V: 175	610	1
$TaVO_5$	32407	FTO/Tec7	0.6	Ta: 68	V: 175	550	3
$V_2Pb_2O_7$	25796	FTO/Tec7	0.6	Pb: 13	V: 180	550	3
$V_2Zn_4O_9$	504923	FTO/Tec7	0.6	Zn: 14	V: 175	550	3
ZrV_2O_7	565725	FTO/Tec7	0.6	Zr: 100	V: 175	550	3

Powder x-ray diffraction (XRD)

The bulk crystal structure and phase distribution of the composition libraries were characterized by XRD using a Bruker DISCOVER D8 diffractometer with Cu K_α radiation from a Bruker IμS source. The XRD measurements were performed on a series of evenly-spaced positions along the composition gradient and collected using a 2D VÅNTEC-500 detector. The images were integrated into 1D patterns and analyzed using DIFFRAC.-SUITE EVA software.

For some composition libraries, XRD data were acquired via a custom HiTp setup incorporated into the bending-magnet beamline 1-5 of the Stanford Synchrotron Radiation Light Source (SSRL) at SLAC National Accelerator Laboratory.[2] The characterization employed a 12.7 keV monochromic source in

reflection scattering geometry with a 2D image detector (Princeton Quad-RO 430 4320). Diffraction images were processed into 1D patterns by WxDiff software.
All the phase identification proceeded by matching the 1D XRD patterns with entries in the International Crystallography Diffraction Database (ICDD).

X-ray Fluorescence (XRF)

The cation compositions in each library were determined by XRF measurements using an EDAX Orbis Micro-XRF system with an x-ray beam approximately 2 mm in diameter. The sensitivity factor for each element was calibrated using commercial XRF calibration standards (MicromatterTM). The oxygen stoichiometry was not specifically controlled or measured in the sputtered composition libraries, that we refer to the ternary oxide compositions as $A_{1-x}B_xO_z$, where x was determined by XRF.

X-ray photoelectron spectroscopy (XPS)

XPS measurements were performed to determine the near-surface chemistry using a Kratos Axis NOVA system with a base pressure of 1×10^{-9} Torr. The x-ray source was a monochromatic Al Kα line at 1486.6 eV. Photoelectrons were collected at 0° from the surface normal with a retarding pass energy of 160 eV for survery XPS scans with a step size of 0.5 eV, and a pass energy of 40 eV for high-resolution core level scans with a step size of 0.025 eV. Data was analyzed using CasaXPS software. To calculate the composition (atomic ratio), a Tougaard background was subtracted. The core level intensities are corrected by the analyzer transmission function and relative sensitivity factors to obtain corrected peak intensities which are used to calculate the atomic ratios.

Photoelectrochemical (PEC) measurements

Scanning droplet cell (SDC) experiments were performed using our previously published instrumentation,[3] which includes a Gamry 600 potentiostat, Ag/AgCl reference electrode, Pt counter electrode, and custom Labview software. Four electrolytes (sodium hydroxide, borate buffer, phosphate buffer, and sulfuric acid) were used at 6 pH values, described in Table S3. Illumination for front side, light-toggled chronoamperometry (CA) measurements at OER potential (1.23 V vs RHE) was provided by four different wavelengths of LEDs ranging from 2 – 3.22 eV (Thor Labs and Doric Lenses LEDC4_385/455/515/595). Photocurrent (I_{photo}) is the difference between the average current during the last two illumination cycles and the current during the dark cycle. CA measurements varied in duration from 4 s to 1800 s with illumination toggled, typically at 0.5 s intervals. Illumination area varied between 0.6 and 1.8 mm^2 and illumination intensity was measured with a photodiode, from which the current density and EQE were calculated, respectively, for each I_{photo}.

Table S3. Summary of electrolytes used in PEC measurements.

pH	Electrolyte
3	0.1 M potassium phosphate monobasic + 0.04 M phosphoric acid + 0.25 M sodium sulfate
7	0.05 M potassium phosphate monobasic + 0.05 M potassium phosphate dibasic + 0.25 M sodium sulfate
9	0.1 M boric acid + 0.05 M potassium hydroxide + 0.25 M sodium sulfate
10	0.1 M boric acid + 0.085 M potassium hydroxide + 0.25 M sodium sulfate
13	0.1 M sodium hydroxide + 0.5 M sodium sulfate
14	1 M sodium hydroxide

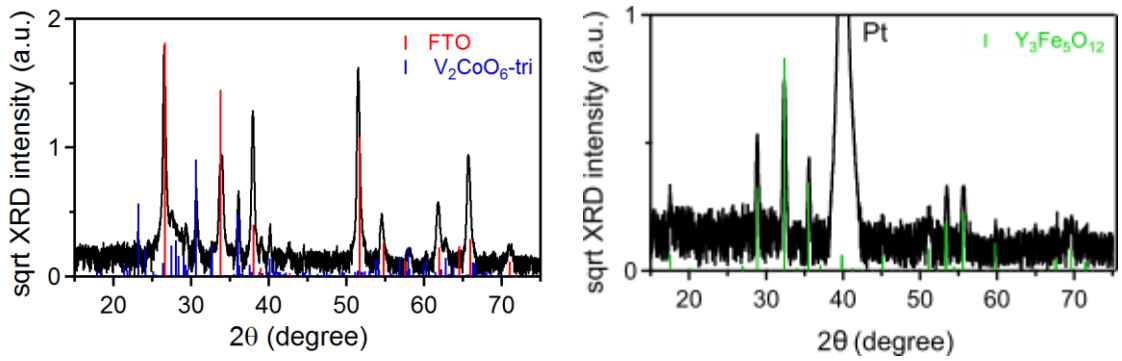

Figure S1. Integrated 1 D XRD patterns of as-prepared (a) V_2CoO_6-tri and (b) $Y_3Fe_5O_{12}$ samples. Besides the strong signals from FTO (red sticks) and Pt (labelled) substrate layer, samples can be identified as triclinic V_2CoO_6 (blue sticks) with space group of P-1 (ICDD: 01-072-1806) and Rhombohedral $Y_3Fe_5O_{12}$ (green sticks) with space group of R-3 (ICDD: 04-014-4007), respectively.

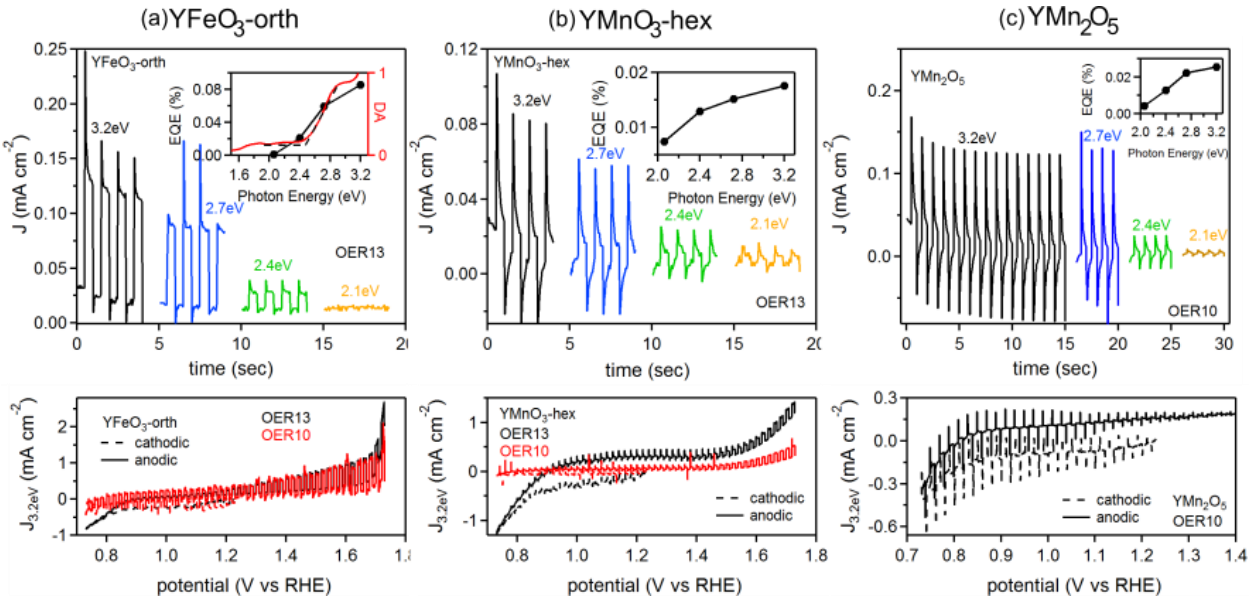

Figure S2. Summary of toggled illumination PEC experiments on (a) $YFeO_3$-orth, (b) $YMnO_3$-hex, and (c) YMn_2O_5, respectively, where transition to higher (lower) current corresponds to toggling illumination on (off). (top) CA at 1.23 V vs RHE with 4 different light sources. (inset) The corresponding spectral EQE. (bottom) CVs with 3.2 eV illumination.

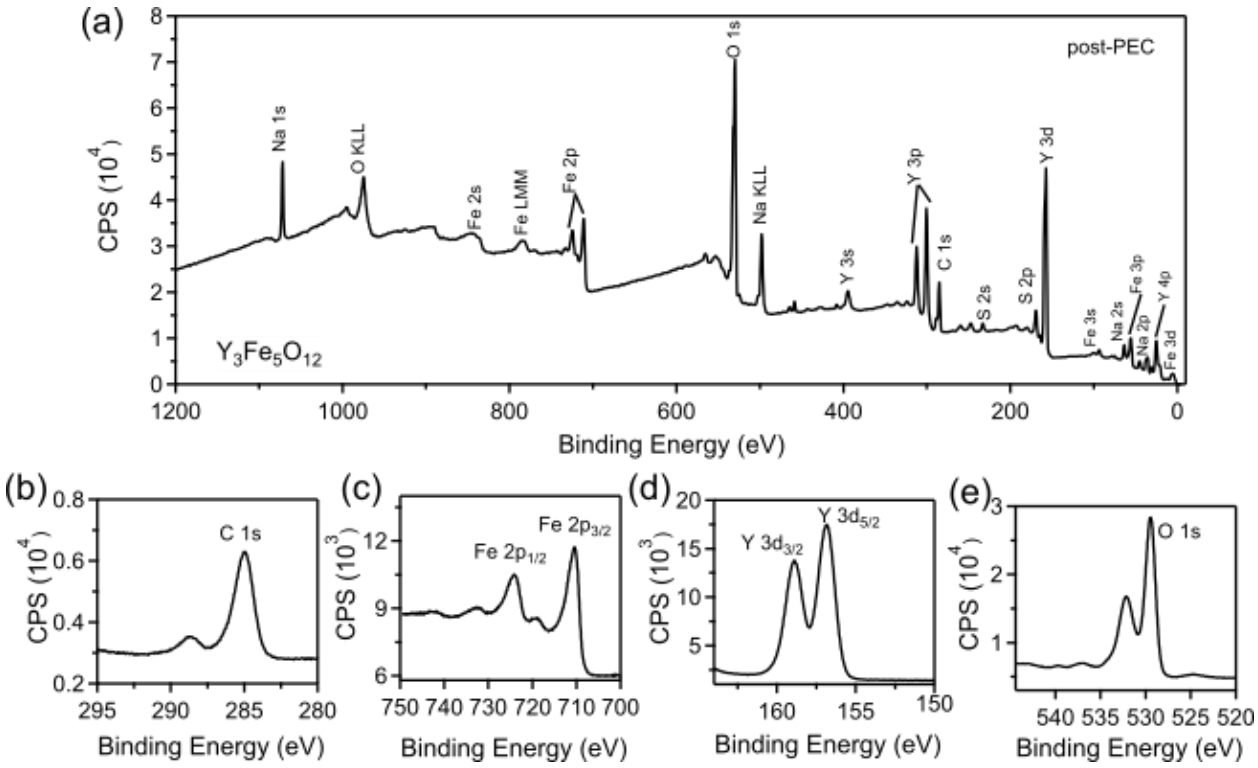

Figure S3. (a) Survey and high-resolution core-level spectra of (b) C 1s, (c) Fe 2p, (d) Y 3d and (e) O 1s of sample $Y_3Fe_5O_{12}$ post PEC measurements at pH 10 and 13 in Figure 1 of maintext. The values of photoelectron binding energy was calibrated to the C 1s peak position of 285 eV. Elemental quantification was performed in the CasaXPS software using a Tougaard background fitting. The composition shows Y/(Y+Fe) of 0.47 in the near-surface.

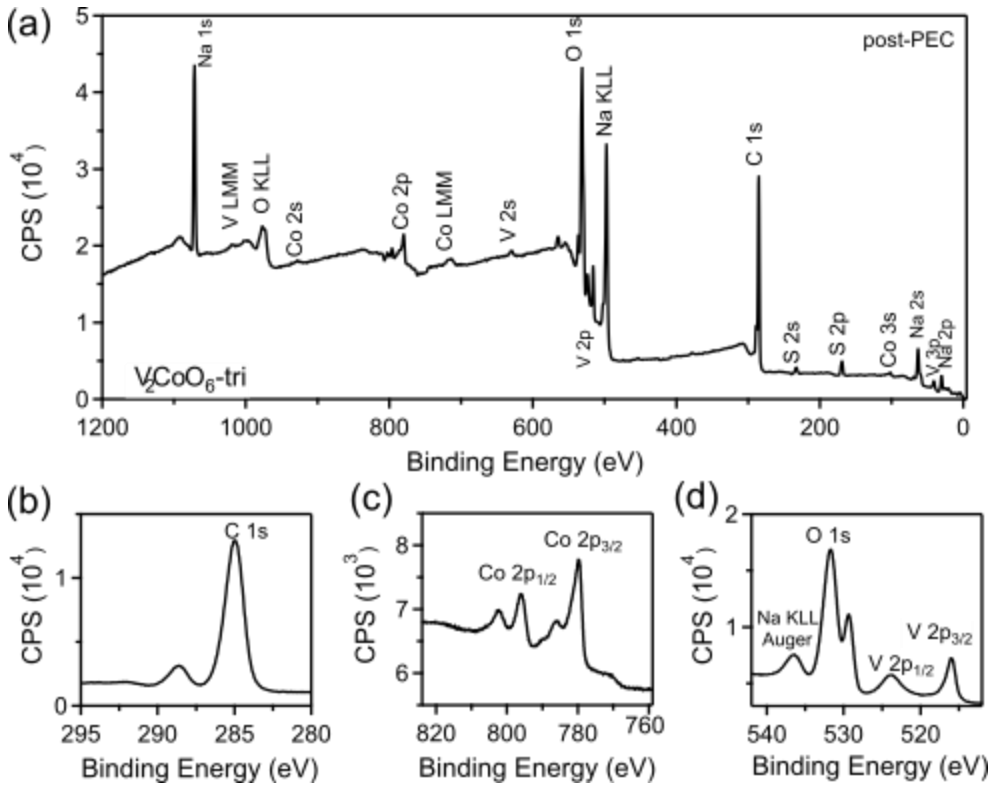

Figure S4. (a) Survey and high-resolution core-level spectra of (b) C 1s, (c) Co 2p, and (d) O 1s of sample V_2CoO_6-tri post PEC measurements at pH9 in Figure 2 of main text. The values of photoelectron binding energy was calibrated to the C 1s peak position of 285 eV. The survey scan confirms the presence of V, Co, and O atoms. Due to precipitation of the electrolyte salt, strong signals from electrolyte-constituent elements Na and S are apparent in the post-photoelectrochemistry survey spectrum. Elemental quantification was performed in the CasaXPS software using a Tougaard background fitting. The composition shows Co/(Co+V) of 0.44 in the near-surface.

$Y_3Fe_5O_{12}$

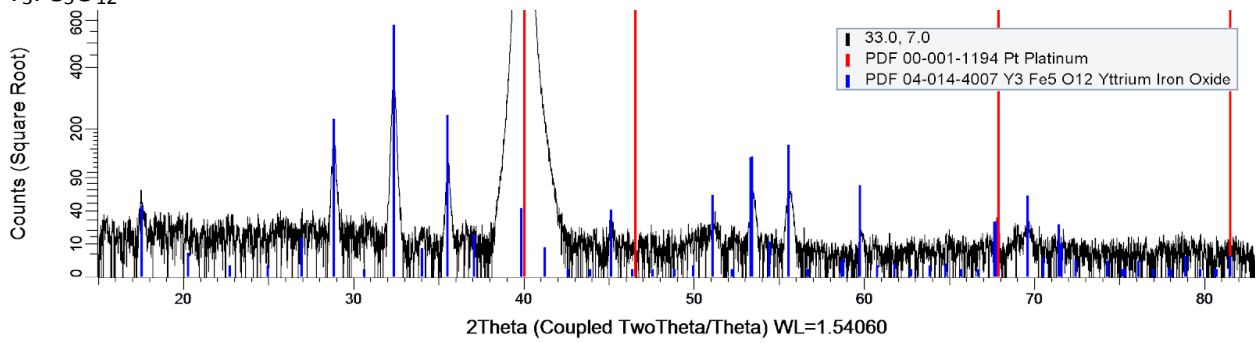

V_2CoO_6-tri

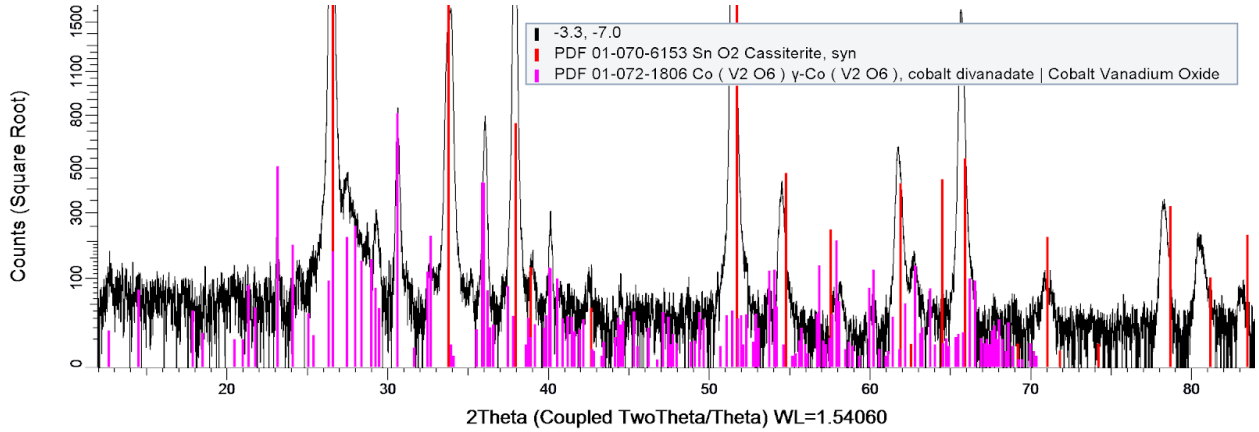

$YMnO_3$-hex

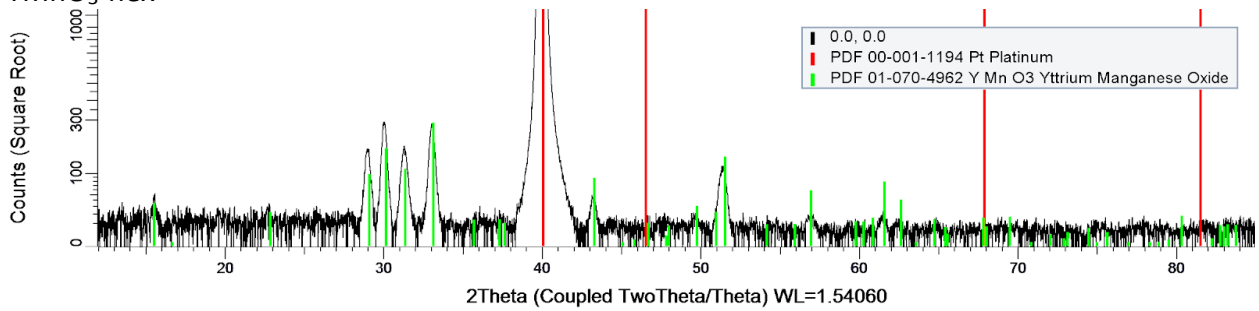

YMn_2O_5

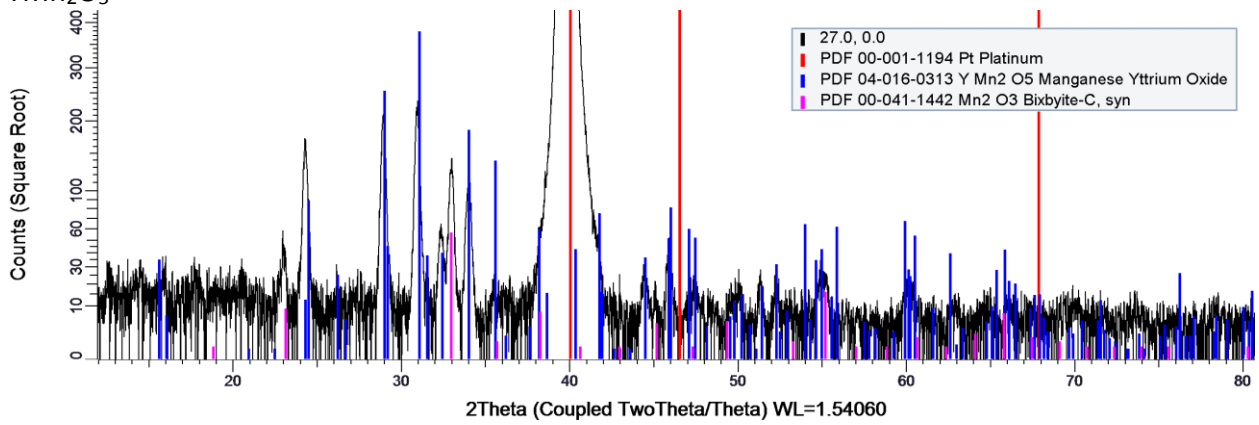

$YFeO_3$-orth

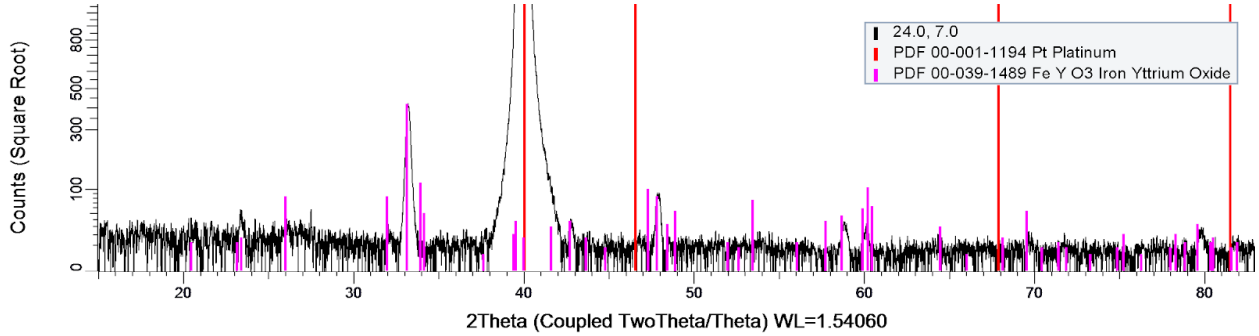

$CaMnO_3$

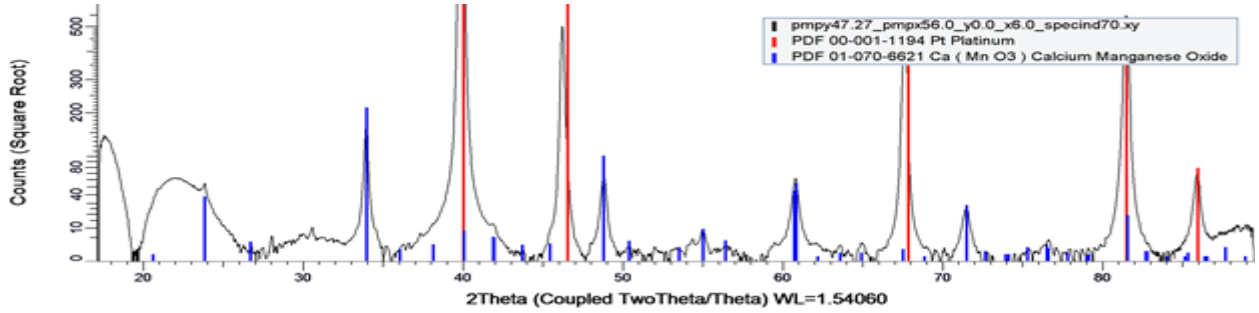

$V(Bi_5O_8)_5$

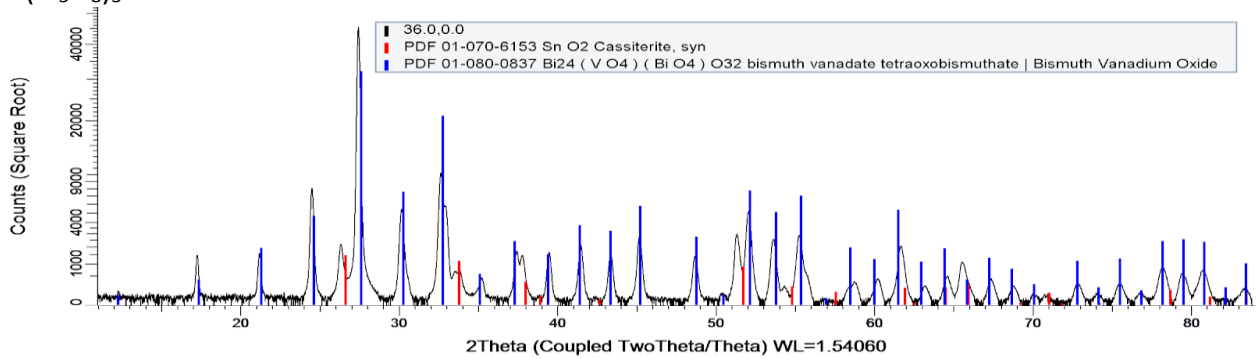

$Nb_{10.7}V_{2.38}O_{32.7}$

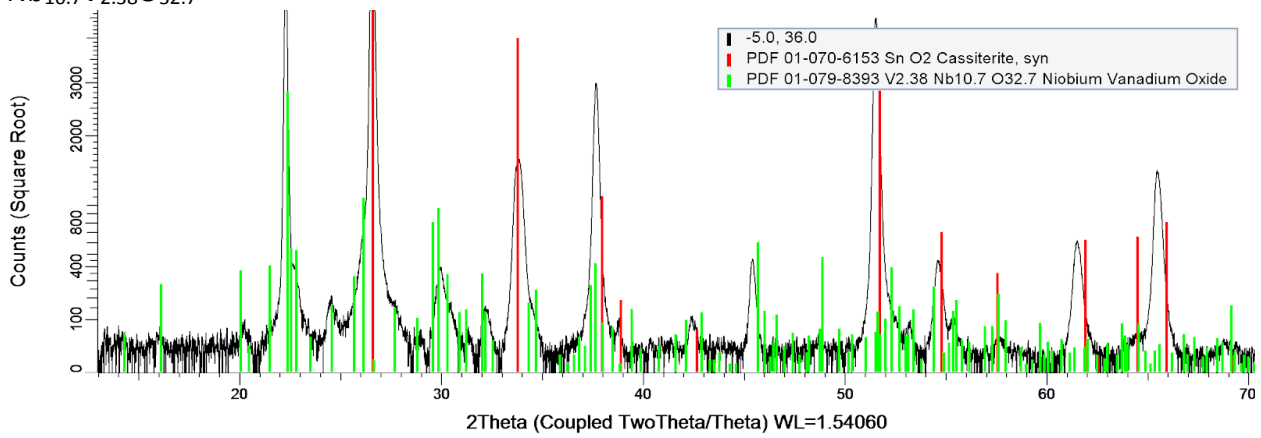

$NbVO_5$

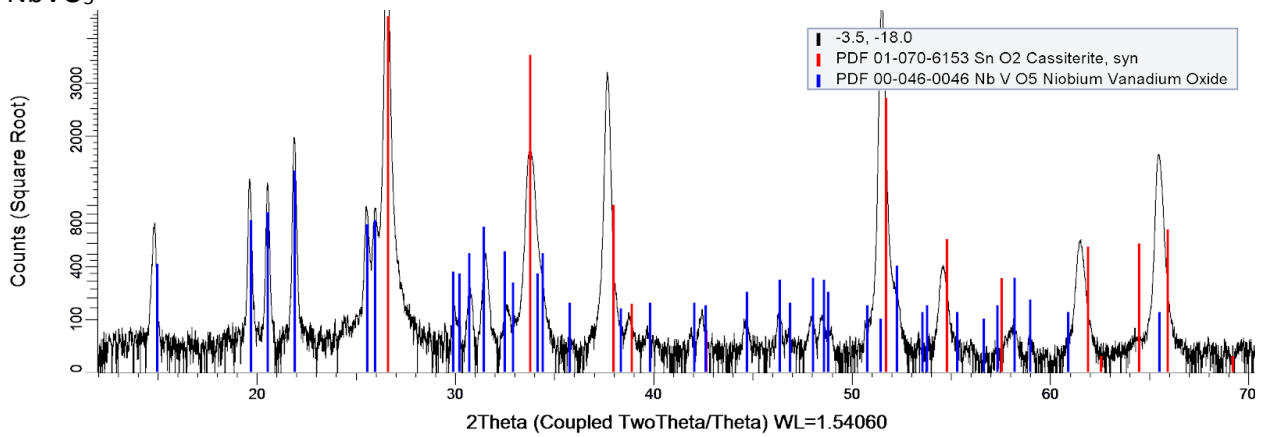

$V_2Pb_4O_9$

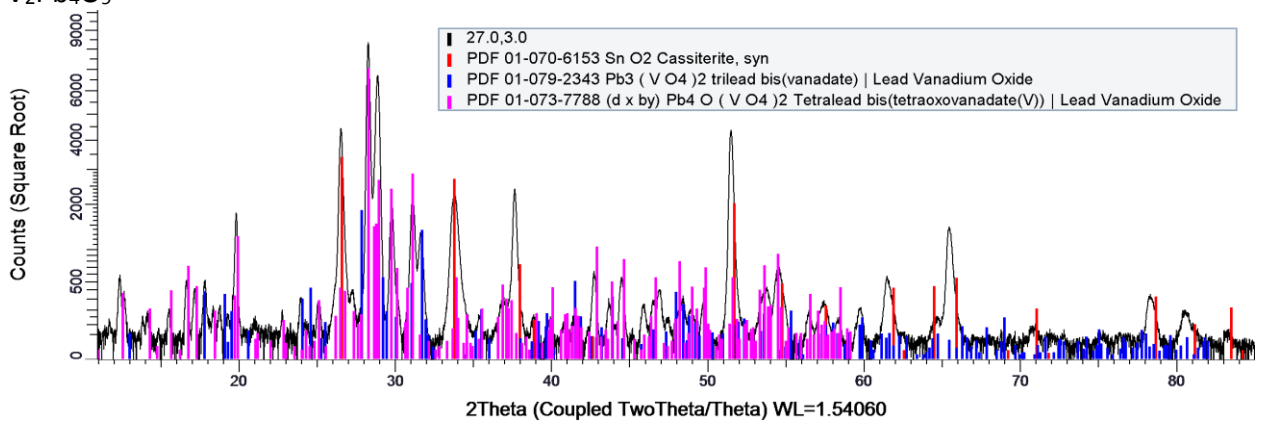

V_2ZnO_6

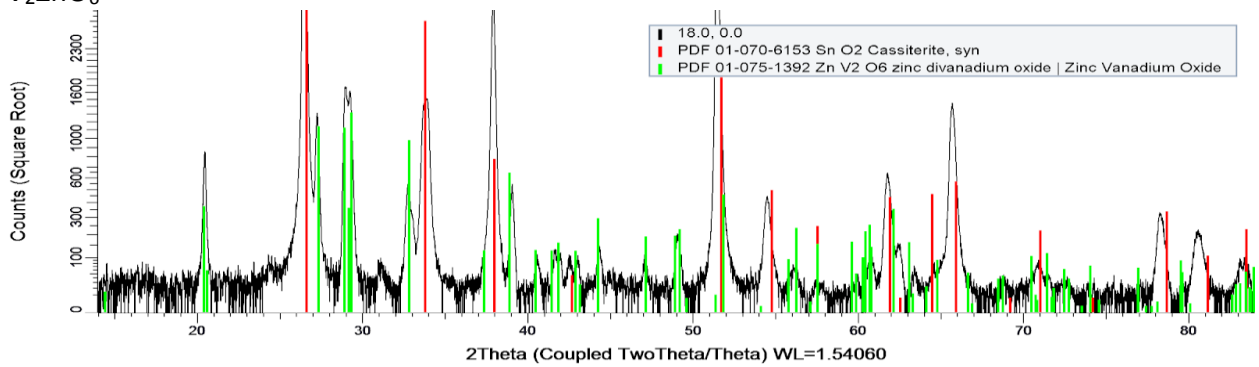

$V_{4.51}Pb_{3.5}O_{14.75}$

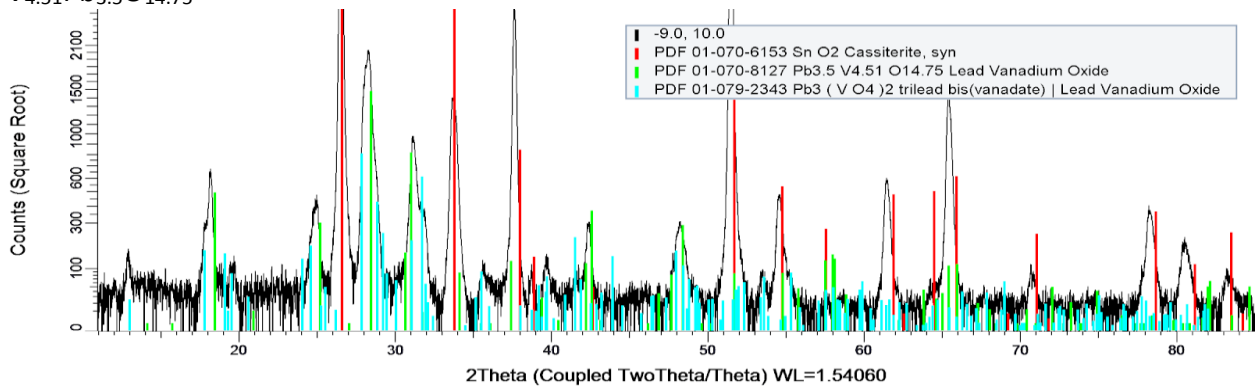

β-$VAgO_3$

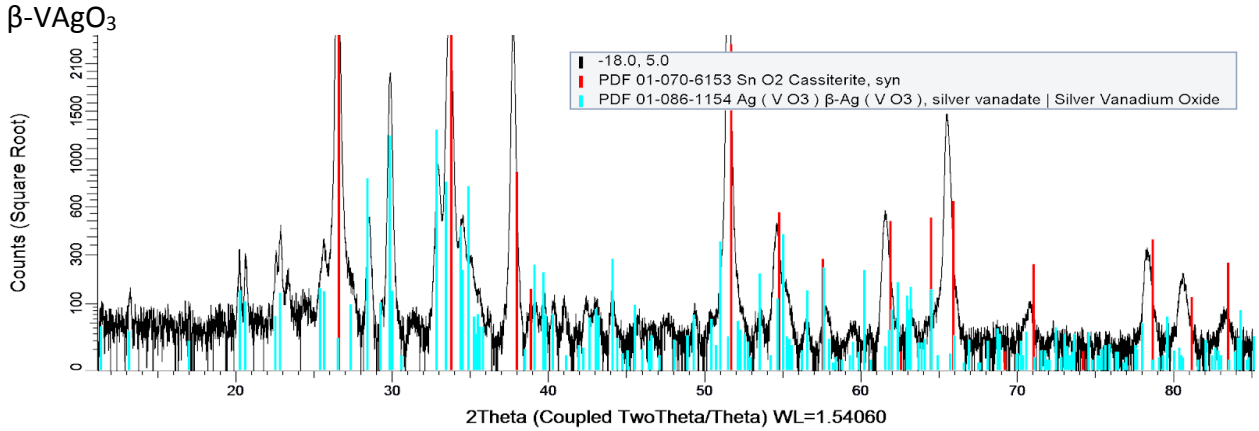

$V_2Ag_{0.333}O_5$

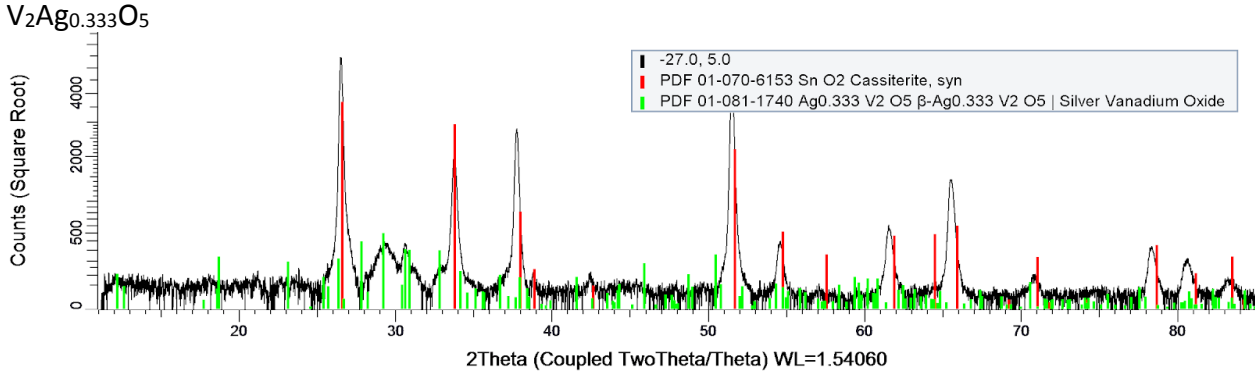

Ca_2MnO_4

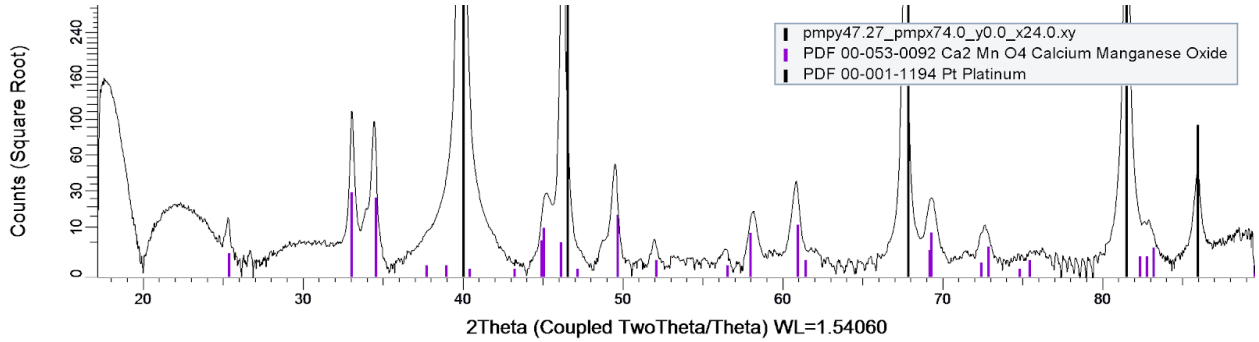

Mn_7SiO_{12}

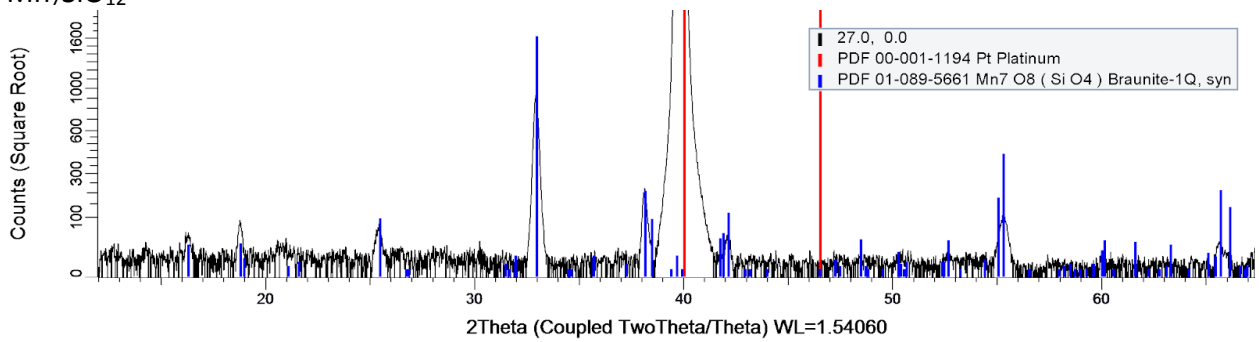

$YMnO_3$-orth

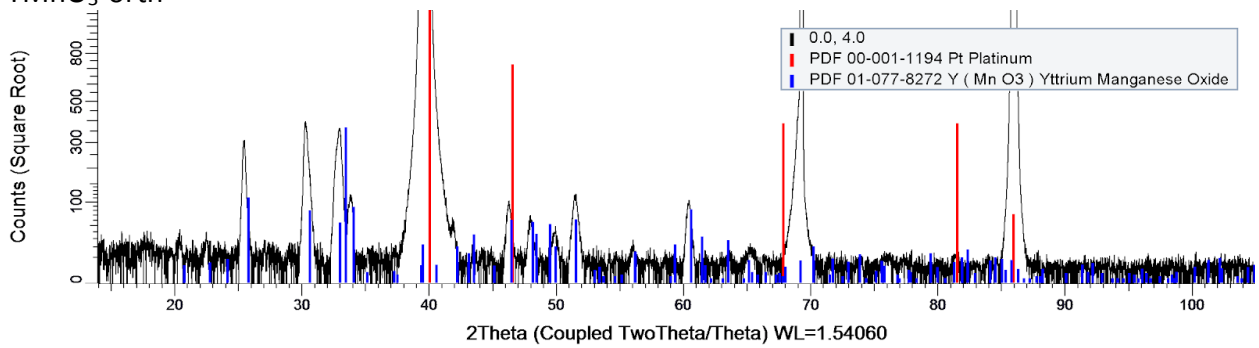

$Mn_{(2/3)}Sb_{(4/3)}O_4$

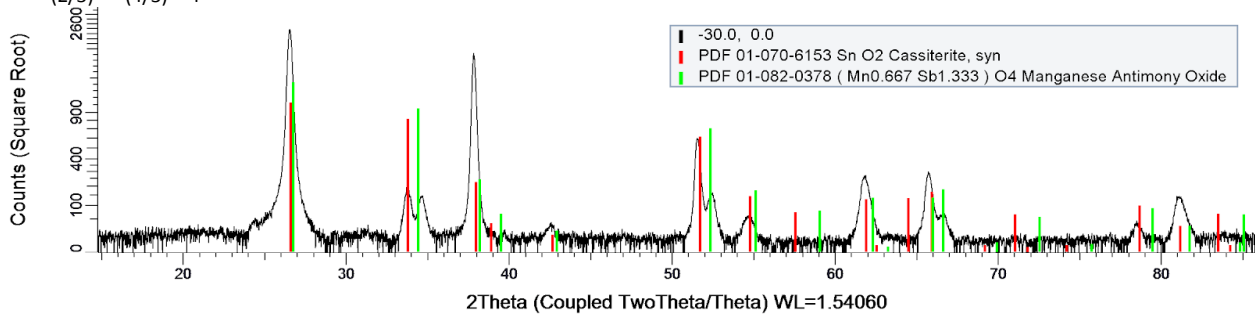

$Ca_2V_2O_7$

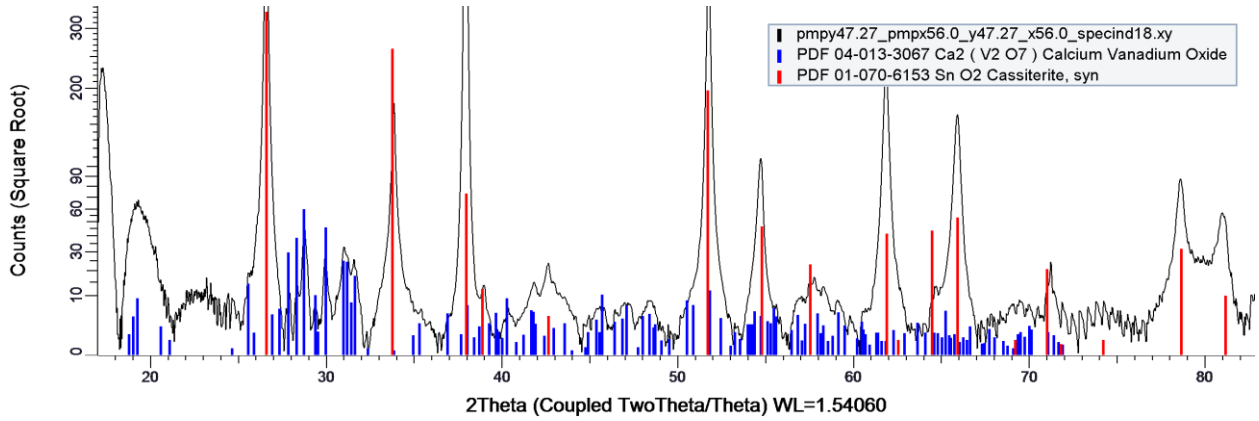

$CaMn_3O_6$

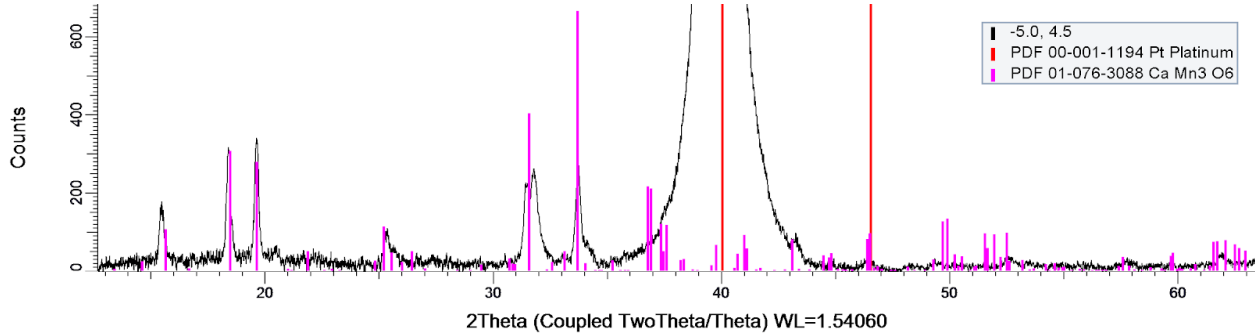

Mg_6MnO_8

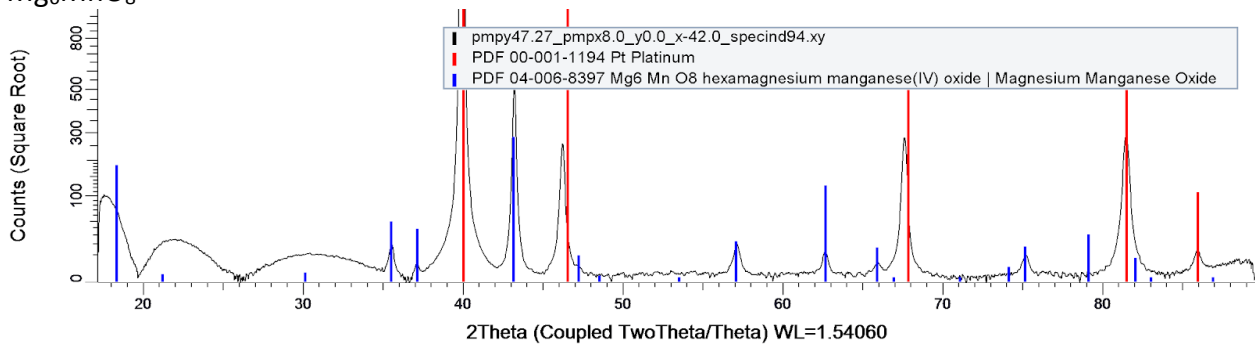

$SrMn_3O_6$

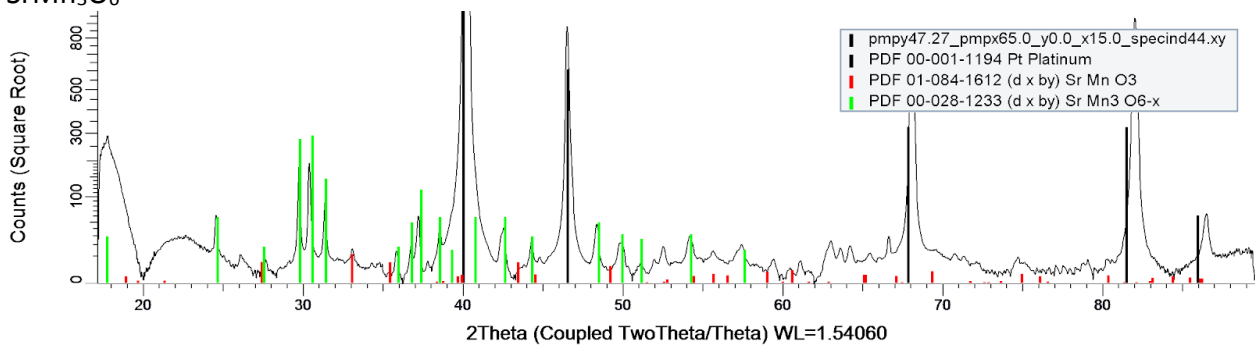

$MnGeO_3$

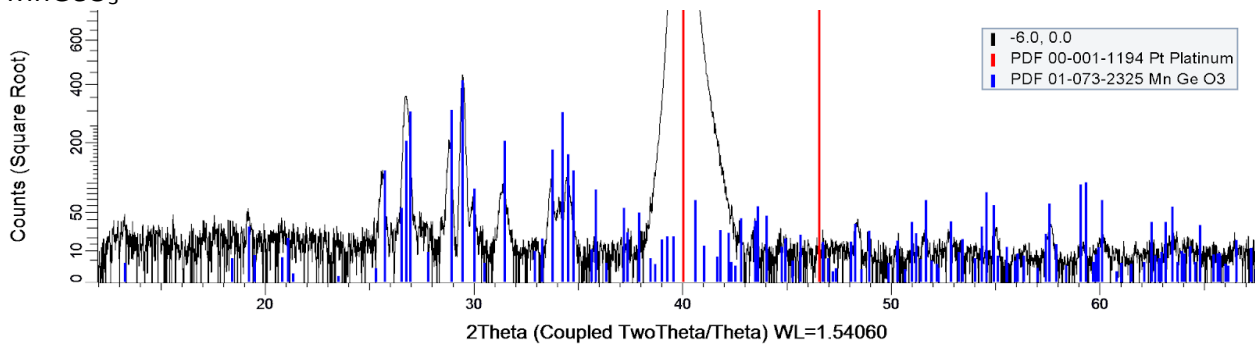

$V_2Bi_8O_{17}$

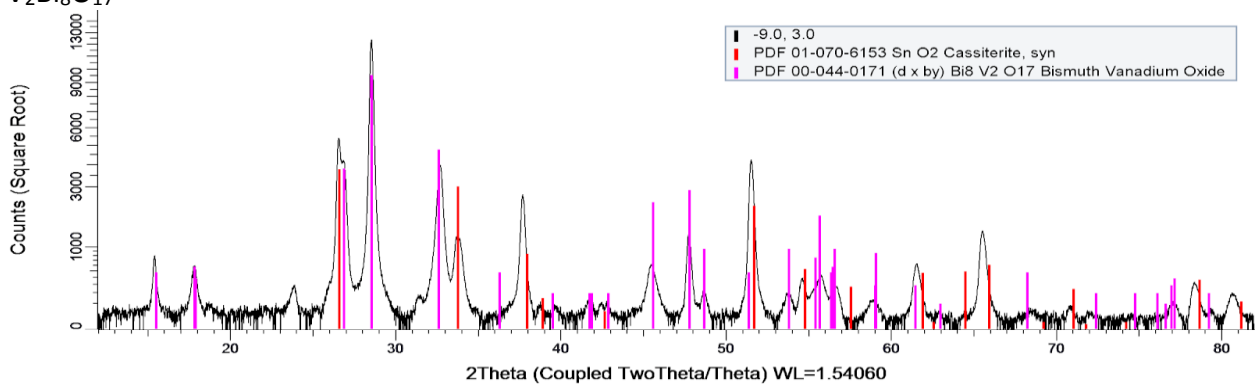

$V_2Bi_{12}O_{23}$

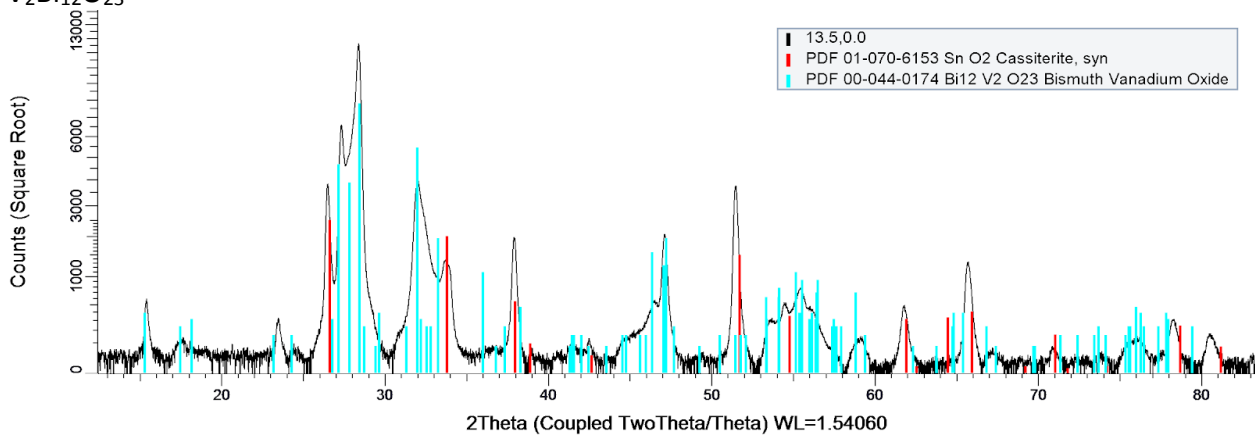

$TaVO_5$

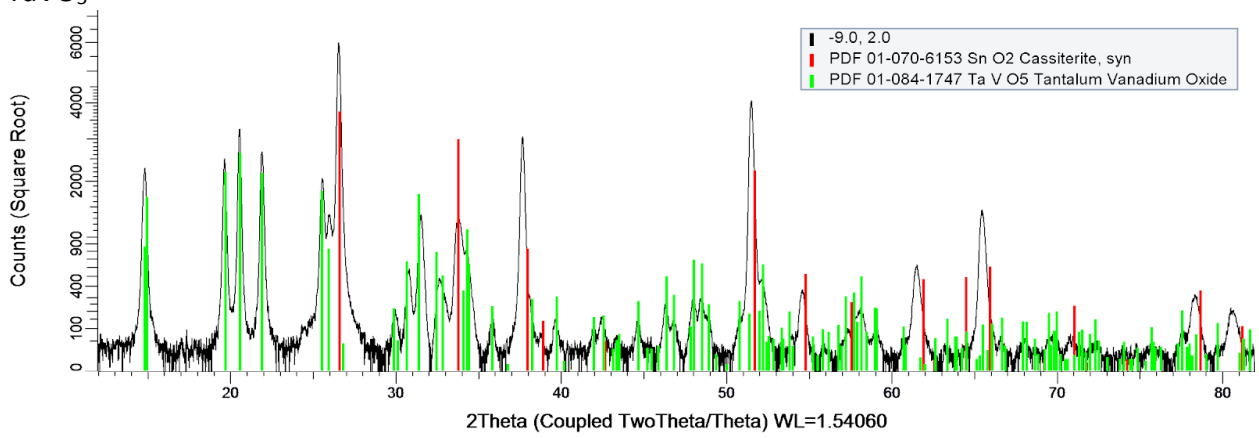

$V_2Pb_2O_7$

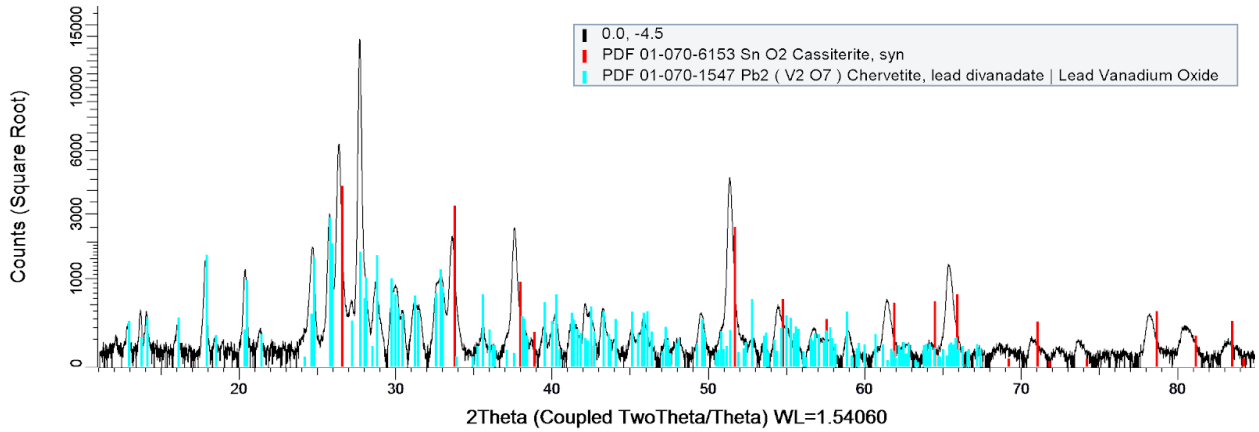

$V_2Zn_4O_9$

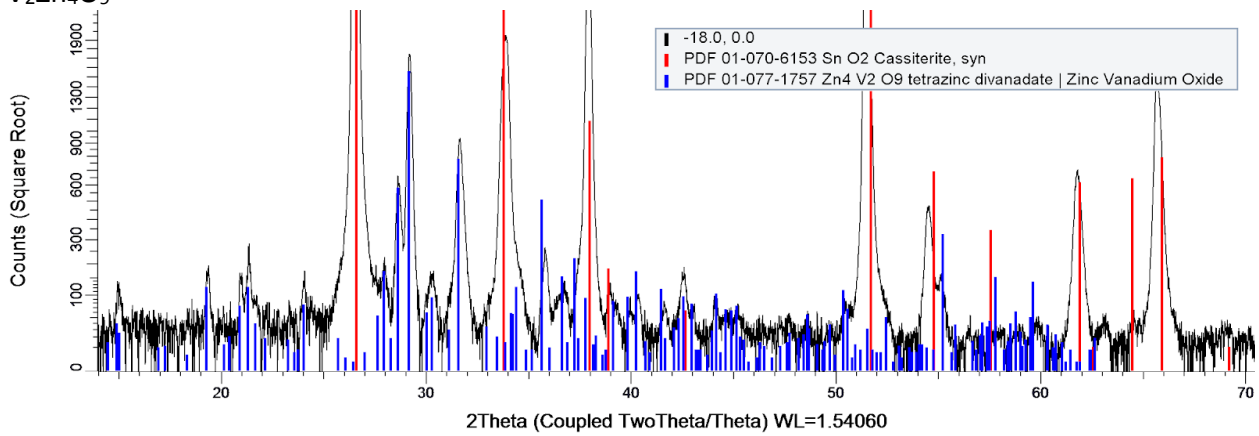

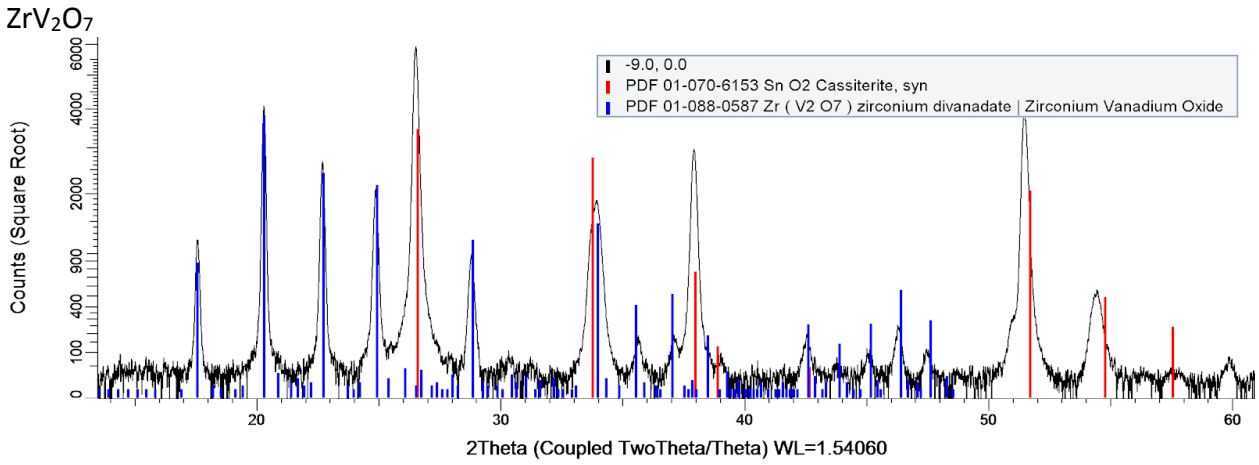

Figure S5. For each XRD pattern, the pattern of the conducting underlayer (Pt or FTO) is shown in red (except for Ca_2MnO_4 and $SrMn_3O_6$, Pt pattern is shown in dark grey) and the pattern of the phase of interest is shown in a different color. The combination of these 2 signals explains all observed XRD peaks, demonstrating phase purity within detectability limits. The least certain phase assignment is for $V_{4.51}Pb_{3.5}O_{14.75}$ where the measured signal best matches this off-stoichiometric phase, although the signal is not strongly differentiated from that of the related entry for the stoichiometric phase $Pb_3(VO_4)_2$.

SI References:

1. S. K. Suram, L. Zhou, N. Becerra-Stasiewicz, K. Kan, R. J. R. Jones, B. M. Kendrick and J. M. Gregoire, *Rev Sci Instrum*, 2015, **86**.
2. J. M. Gregoire, D. G. Van Campen, C. E. Miller, R. J. R. Jones, S. K. Suram and A. Mehta, *J Synchrotron Radiat*, 2014, **21**, 1262-1268.
3. J. M. Gregoire, C. X. Xiang, X. N. Liu, M. Marcin and J. Jin, *Rev Sci Instrum*, 2013, **84**.